Elucidation of a nutlin-derivative—HDM2 complex structure at the interaction site by NMR molecular replacement: A straightforward derivation

Journal of Magnetic Resonance Open 10-11 (2022) 100032

Contents lists available at ScienceDirect

Journal of Magnetic Resonance Open

journal homepage: www.sciencedirect.com/journal/journal-of-magnetic-resonance-open

Elucidation of a nutlin-derivative—HDM2 complex structure at the interaction site by NMR molecular replacement: A straightforward derivation

Valerie Mertens [a], Marie Jose Abi Saad [b], Nicolas Coudevylle [b], Marielle Aulikki Wälti [a], Aaron Finke [c], May Marsh [c], Julien Orts [b,*]

[a] ETH, Swiss Federal Institute of Technology, Laboratory of Physical Chemistry, Vladimir-Prelog-Weg 2, CH-8093 Zürich, Switzerland
[b] University of Vienna, Department of Pharmaceutical Sciences, Althanstrasse 14, A-1090 Vienna, Austria
[c] Swiss Light Source, Paul Scherrer Institute, CH-5232 Villigen, Switzerland

ARTICLE INFO

Keywords:
NMR molecular replacement
Complex structure
Drug design
NMR spectroscopy
Structure elucidation

ABSTRACT

Protein—ligand complex structures are key in structure-based drug discovery, but their derivation largely relies on X-ray crystallography. While NMR is able to provide atomic resolution complex structures, traditional NMR structure calculation methods are too slow for drug discovery timelines. We recently developed the NMR molecular replacement (NMR^2) method that substantially reduces the time needed to derive protein—ligand complex structures, mainly by bypassing the laborious protein sequential resonance assignment step. Here we show how we applied NMR^2 to derive the structure of the protein HDM2 in complex with the small molecule caylin-1, an analog of nutlin, based on the HDM2—nutlin complex structure that was already derived by NMR^2. This study illustrates how sparse information from a previous NMR^2 structure elucidation can be employed to efficiently determine further protein-analog complex structures. We think NMR^2 has the potential to become a major tool in structure-based drug discovery, especially when X-ray crystallography is difficult to implement.

1. Introduction

We recently established a new methodology in NMR spectroscopy, called NMR molecular replacement (NMR^2), that derives protein—ligand complex structures at the interaction site without the need to assign the protein and solely relying on a predefined algorithm [1]. NMR^2 is a fast, robust and automated structure calculation process. We have demonstrated that the NMR^2 methodology can generate ligand-protein complex structures useful for structure-based drug discovery (SBDD) for a variety of ligand types covering fragments, drug-like molecules and peptides, with affinities in the nanomolar to millimolar range [1–5]. During a structure-based drug design campaign, typically several structures of analogous compounds have to be derived. In this study we illustrate on the system HDM2—nutlin/caylin, two analogous compounds, how NMR^2 can easily and efficiently derive the structure of a protein in complex with a small molecule ligand if the NMR^2 structure of a protein-analog complex is available.

HDM2 is a human oncogenic protein that efficiently binds the tumor suppressor p53 and, when over-expressed in tumors, inhibits p53. HDM2 binds p53 via a well-defined N-terminal hydrophobic pocket, which is, in the HDM2-p53 complex, occupied by three side-chains Phe19, Trp23 and Leu26 of the p53 peptide [6,7]. Targeting this protein-protein interface is considered a promising therapeutic strategy for the treatment of human cancers that express wild-type p53 and tremendous research is performed to find effective inhibitors [8–12]. The first class of potent and selective small-molecules found to inhibit this interaction is a series of cis-imidazoline analogs, called nutlins (Fig. 1a)[13–16]. Several prominent representatives of this group have successfully entered clinical trial as potential anti-cancer agents [17,18]. The 3D structure of the HDM2—nutlin-3a binding interface has already been solved by NMR^2 and X-ray crystallography (PDB code 5C5A) [1]. It was reported that the NMR^2 HDM2—nutlin-3a structure slightly differs from the ones previously derived by X-ray crystallography at the Phe19 pocket (supplementary Fig. S1). The difference was attributed to the crystal packing interfaces that involved the ligand and the ligand binding site protein residues. Crystalizing the complex in a different space group (PDB 5C5A) resulted in a complex structure identical to the one derived by NMR^2.

* Corresponding authors.
E-mail addresses: may.sharpe@psi.ch (M. Marsh), julien.orts@univie.ac.at (J. Orts).

https://doi.org/10.1016/j.jmro.2022.100032
Received 30 November 2021; Received in revised form 6 January 2022; Accepted 9 January 2022
Available online 14 January 2022

Caylin-1 is an analog of the high-affinity HDM2-inhibitor nutlin-3a that contains an additional chlorine substituent at the 3′ position of two of the phenyl rings (Fig. 1b). Similar to nutlin-3a, caylin-1 has been shown to bind HDM2 with high affinity and is therefore a system well-suited for evaluating the *N*MR[2] performance when deriving complex structures of protein-small molecule analogs. Here we report the *N*MR[2] structure of caylin-1 in complex with HDM2, derived using additional information from the previously *N*MR[2]-derived HDM2—nutlin-3a complex structure. The described approach benefits the *N*MR[2] users and finds application in structure-based drug design.

2. Experimental section

2.1. Small molecules

Caylin-1 and nutlin-3a were purchased from Cayman Chemical, with a purity above 98% and validated by ^{1}H NMR.

2.2. Protein expression and purification

Recombinant production and purification of uniformly [^{13}C,^{15}N]-labeled HDM2(15–111) was performed as previously described [1]. Purified HDM2(15–111) was stored at −80°C in storage buffer (50 mM Tris-HCl, 200 mM NaCl, 1 mM TCEP, 1 mM EDTA, 10% glycerol at pH 7.5 in H_2O).

2.3. NMR sample preparation

For NMR experiments to assign the free ligand, a sample with a concentration of 1 mM caylin-1 in 100% dimethyl sulfoxide (DMSO) was prepared. NMR samples for titration were produced by exchanging the storage buffer of purified HDM2(15–111) into NMR buffer (25 mM phosphate buffer, 25 mM NaCl, 0.1 mM EDTA, 2 mM TCEP at pH 6.5 in H_2O) using a PD-25 column (GE Healthcare). A 50 mM stock-solution of caylin-1 in d_6-DMSO was used to prepare a series of ten NMR samples with a protein concentration of 100 µM and ligand concentrations of 0, 20, 50, 75, 100, 150, 200, 300, 400 and 500 µM. All samples were prepared with a total of 3% DMSO to compensate for the DMSO added with the ligand. For the measurement of intra- and inter-molecular NOE buildup curves the storage buffer was exchanged into NMR buffer (25 mM phosphate buffer, 25 mM NaCl, 0.1 mM deuterated EDTA, 2 mM deuterated TCEP at pH 6.5 in D_2O) using a PD-25 column (GE Healthcare). Caylin-1 was dissolved in d_6-DMSO and added to the protein with a final protein:ligand ratio of 1:1.2. The complex was concentrated to a final protein concentration of 425 µM.

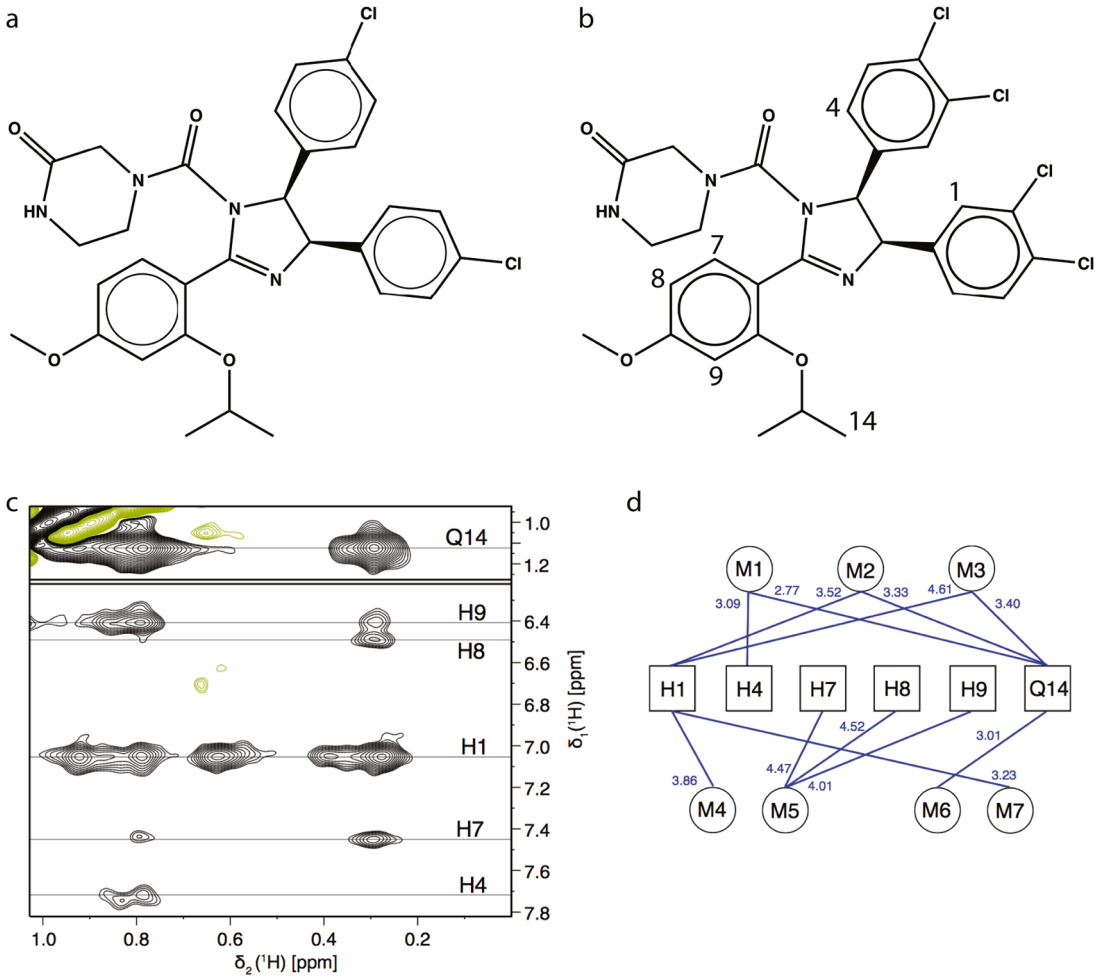

Fig. 1. NOE-derived intermolecular distance restraints between HDM2 and caylin-1. Chemical structures of nutlin-3a (a) and caylin-1 (b). (c) F_1-[^{13}C,^{15}N]-filtered 2D [^{1}H,^{1}H]-NOESY spectrum (τ_{mix} = 100 ms) showing intermolecular cross-peaks between caylin-1 and unassigned methyl groups of HDM2. Ligand resonance positions are marked by horizontal lines and are assigned according to the numbering scheme given in (b) and supplementary Fig. S2; (d) NOE-derived intermolecular distance restraint network of the HDM2-caylin-1 complex. Unassigned methyl groups of HDM2 are arbitrarily designated M1-M7. The derived upper distance limits between individual protein and ligand protons are reported in Å.

2.4. NMR measurements

All NMR experiments were carried out at 288.15 K on a Bruker 600 MHz or 700 MHz ^{1}H frequency spectrometer equipped with a triple resonance cryoprobe. All spectra were processed with TopSpin 3.2 (Bruker) and subsequently evaluated using ccpNMR 2.4.2 [19].

To assign the free caylin-1 in DMSO, the following spectra were recorded at the 600 MHz spectrometer: 1D ^{1}H NMR spectrum with 32,768 points and 128 scans; a 2D [^{1}H,^{1}H]-DQF-COSY, a 2D [^{1}H,^{1}H]-NOESY and a 2D [^{1}H,^{1}H]-TOCSY each with 768(t_1)x16,384(t_2) points, an inter-scan delay of 2.0 s and 8 scans per increment, a $t_{1,max} = 63.9$ ms and a $t_{2,max} = 1136$ ms (supplementary Fig. S2).

Titration of caylin-1 to HDM2(15–111) was followed on the 700 MHz spectrometer recording a series of ten 2D [^{15}N,^{1}H]-HSQC spectra with a total of 128(t_1)x2048(t_2) points ($t_{1,max}$(^{15}N) = 28.2 ms, $t_{2,max}$(^{1}H) = 104.4 ms). A total of 24 scans were acquired per time-increment and the recycle delay was set to 1.0 s. For the ^{1}H resonance assignment of caylin-1 bound to HDM2(15–111), a F_1,F_2-[^{13}C,^{15}N]-filtered 2D [^{1}H,^{1}H]-TOCSY with 512(t_1)x4096(t_2) points ($t_{1,max}$ = 35.5 ms, $t_{2,max}$ = 239.2 ms), an interscan delay of 0.8 s and 256 scans per increment was recorded on a 600 MHz spectrometer. A F_1-[^{13}C,^{15}N]-filtered 2D [^{1}H,^{1}H]-NOESY spectrum ($\tau_{mix} = 100$ ms) was also used (seee below and supplementary Fig. S3) [20].

2.5. NMR^2 structure determination

A series of four 2D F_1-[^{13}C,^{15}N]-filtered [^{1}H,^{1}H]-NOESY spectra with mixing times τ_{mix} = 40, 60, 80, and 100 ms were recorded on the 700 MHz spectrometer Bruker, in an interleaved mode for the measurement of ligand intra- and protein-ligand intermolecular NOE buildup curves. The pulse sequence noesygpphwgx1 was used with a water presaturation during the mixing time instead of the watergate. [^{13}C,^{15}N]-filtering along F_1 was performed using two consecutives [^{13}C,^{15}N]-purged sweep filter blocks with frequency-matched WURST inversion pulses on the ^{13}C-channel. The first WURST pulse for purging was centered at 0 ppm, covering a 60 kHz sweep range with a linear sweep rate of 3.9×10^7 Hz/s, with a pulse length of 1.54 ms and $B_{1,max}$ of 5 kHz. The second WURST pulse for purging was centered at 0 ppm, covering a 60 kHz sweep range with a linear sweep rate of 3.1×10^7 Hz/s, with a pulse length of 1.94 ms and $B_{1,max}$ of 5 kHz. A total of 4096(t_2)x600(t_1) points were recorded with $t_{2,max}$ = 225.2 ms and $t_{1,max}$ = 33.0 ms. For each time-increment, 176 scans were acquired with an inter-scan delay of 0.8 s [20].

Fitting of diagonal-peak intensity decay curves and cross-peak intensity build-up curves for the extraction of inter-spin upper distance limits was performed with the software package eNORA using a simple two-spin system model [21]. The auto-relaxation rates, ρ_i, and initial magnetizations, $\Delta M_{ii}(0)$, were determined using a mono-exponential decay function, $\Delta M_{ii}(t) = \Delta M_{ii}(0)\exp(-\rho_i t)$. The cross-relaxation rates, σ_{ij}, were fitted following a two-spin system approximation model for the protein–ligand NOEs, $\Delta M_{ij}(t)$, Eq. (1). The corresponding distances, r_{ij}, were derived from the cross-relaxation rates, σ_{ij}, defined in Eq. (3),

$$\frac{\Delta M_{ij}(t)}{\Delta M_{ii}(0)} = -\frac{\sigma_{ij}}{(\lambda_+ - \lambda_-)}\left(e^{-\lambda_- t} - e^{-\lambda_+ t}\right) \quad (1)$$

$$\lambda_\pm = \frac{\rho_i + \rho_j}{2} \pm \sqrt{\left(\frac{\rho_i - \rho_j}{2}\right)^2 + \sigma_{ij}^2} \quad (2)$$

$$\sigma_{ij} = \frac{b^2}{r_{ij}^2}(6J(2\omega) - J(0)) \quad (3)$$

$$J(\omega) = \frac{2}{5}\left(\frac{\tau_c}{1 + (\omega\tau_c)^2}\right) \quad (4)$$

$$b = \frac{1}{2}\frac{\mu_0}{4\pi}\hbar\gamma_H^2 \quad (5)$$

where μ_0 is the permeability of vacuum, $\hbar$ the reduced Planck constant, γ_H the gyromagnetic ratio of the nucleus, and τ_c the rotational correlation time of the protein, 10.5 ns, derived from the ^{15}N-T_1, ^{15}N-$T_{1\rho}$ relaxation rates using the software TENSOR2 [22].

Structure calculations of the bound ligand were carried out with the software CYANA and the *NMR*^{2} software package was then used to calculate the structure of the complex binding pocket [3,23]. Finally, UCSF Chimera was used to visualize and evaluate the calculated ligand- and complex structures.

2.6. Cocrystallization of HDM2 with caylin-1

Purified HDM2(15–111) was diluted to 0.1 mM with 50 mM Tris pH 7.5, 200 mM NaCl, 1 mM TCEP, 1 mM EDTA, and 10% glycerol. Caylin-1 was added to the 0.1 mM HDM2 solution in 2-fold excess and incubated overnight at 4°C. Subsequently, for crystallization trials, the solution was concentrated to reach a final protein concentration of 1 mM. Initial crystallization screens were dispensed using a TTP Mosquito LCP robot (TTP LabTech) using SwissCI 2-drop vapor diffusion plates. Drop sizes of 200 nL reservoir and 200 nL protein were used. Crystals were obtained in the ammonium sulfate screen from Qiagen containing 2.0 M sodium chloride and 2.0 M ammonium sulfate. A seed stock was made from these crystals. This was then used to seed into a grid screen of 2.0 M–3.0 M ammonium sulfate and 100 mM MES pH 6.0. These drops were setup manually using 24 well sitting drop Cryschem plates from Hampton Research. Drop sizes of 1μL reservoir, 1μL protein and 0.5 μL seed stock were used.

Crystals appeared within 2 days under a condition containing 0.1 M MES pH 6.0 and 2.8 M ammonium sulfate.

2.7. X-ray data collection and structure determination

For data collection, crystals were cryoprotected in 80% saturated lithium sulfate and flash-frozen in the cold N_2 stream. Diffraction data were collected at 100 K using the beamline X06DA of the Swiss Light Source. A total of 180° of data were collected at a wavelength of 1.0 Å with 0.1° oscillation and 0.1 s exposure. Data were processed using XDS to 1.26 Å. Processing statistics are shown in Table S1. The structure was solved using molecular replacement with Phaser using the protein with PDB code 5C5A as a model. Refinement was carried out with phenix-refine and model rebuilding was carried out in Coot [24,25]. Iterative rounds of model building and refinement yielded the final structure. The refinement statistics are shown in supplementary Table S1. The structure was deposited in the Protein Data Bank with accession code: 7QDQ.

3. Results and discussion

In its apo form, HDM2(15–111) exhibits a [^{15}N,^{1}H]-HSQC spectrum with more than 200 observable peaks (supplementary Fig. S4), revealing the presence of at least two different protein conformations for apo-HDM2 [26]. Upon addition of increasing amounts of caylin-1, the majority of protein amide signals gradually disappears while numerous new signals appear (supplementary Fig. S4). In the presence of an excess of caylin-1, only one set of resonances is observed. The titration experiment reveals that the HDM2—caylin-1 complex is already fully saturated at a protein:ligand ratio of ~1:1, confirming caylin-1 as a high-affinity binder of HDM2 and providing the optimal protein:ligand ratio for experiments related to the *NMR*^{2} structure determination. A detailed description of the *NMR*^{2} structure determination procedure and associated NMR experiments is given in [1].

Based on NOE build-up curves obtained from a series of F_1-[^{13}C,^{15}N]-filtered [^{1}H,^{1}H]-NOESY experiments, we determined a total of 18 intra-ligand and 12 inter-molecular distance restraints between caylin-1 and 7 unassigned HDM2 methyl groups arbitrarily labeled M1-M7 (Fig. 1d, details on the ^{1}H resonance assignment of HDM2-bound caylin-1 are

given in the SI).

We used these distance restraints with *N*MR^2 in order to solve the solution structure at the interface of the HDM2—caylin-1 complex. The input structure of HDM2 required by *N*MR^2 was extracted from the HDM2-nutlin3a complex (PDB code 5C5A) [1]. Further, based on the available information on the HDM2-nutlin-3a complex and due to the high similarity between the two ligands, the ligand-binding site on the protein could be specified and protein methyl group M5 could be assigned unambiguously prior to the structure calculation procedure. The *N*MR^2 complex structure calculation converged after 3 cycles and a total number of 198,709 structure calculations, corresponding to ~110 core-hours. Compared to the HDM2-nutlin-3a complex (17,919,188 structure calculations), the number of structure calculations, thus computing time, could be reduced by a factor of 90 simply due to the additional information derived from the known structure of an analogous complex [1]. In addition to the gain of speed, only upper limit distance restraints were employed in the *N*MR^2 calculations, rendering the calibration of the NOESY cross peaks less critical.

Among the first 10 best *N*MR^2 structures, 7 HDM2-caylin-1 complex structures, including the top ranked one, show a highly similar binding mode with a heavy-atom rmsd of 1.15 Å, after superposition of the protein. This illustrates that the *N*MR^2 structure calculation process is robust and delivers among the top ranked complexes the ones that correspond to similar protein assignments, namely the assignment combinations of the prochiral methyl carbons of the leucines and valines. Since several valine and leucine residues are present in the binding site and could interact with caylin, it is expected to have multiple prochiral methyl assignment combinations that potentially fulfill the NMR data without significantly modifying the complex structure. The *N*MR^2 HDM2—caylin-1 structure, i.e. the structure with the least number of violations, converged with a final target function of 0.65 Å^2 for the distance restraints and 0.58 Å^2 for the repulsive van-der-Waals violations. The binding mode of caylin-1 recapitulates the three crucial hydrophobic interactions of the native p53/HDM2 complex, with the two dichlorophenyl and the dimethyl groups populating the three subpockets of the protein (Fig. 2).

The structure of the HMD2—caylin-1 complex solved with *N*MR^2 shows good agreement with the HDM2—caylin-1 structure determined by X-ray crystallography (Fig. 2) as represented by a rmsd of 0.80 Å (X-ray conformation 1) or 0.92 Å (X-ray conformation 2) on ligand heavy atoms after superposition of the protein. Interestingly, X-ray crystallography reports two equally populated structures at 100 K, while the *N*MR^2 structure converged to only one conformation at 288.15 K. Despite these differences, the core of the ligand, the imidazoline ring and the three hydrophobic moieties interacting with the protein are overlapping with sub-angstrom rmsd.

4. Conclusion

In a structure-based drug design campaign, several structures of analogous compounds have to be determined during the successive rounds of ligand optimization. While NMR is the method of choice for the rapid screening of large libraries of ligands, it fails to deliver atomic resolution complex structures within a timeframe compatible with drug discovery timelines. Our recently developed NMR molecular replacement (*N*MR^2) method dramatically reduces the time needed to derive protein—ligand complex structures, thus allowing to solve protein—ligand structures within the timeframe of a typical drug design campaign. Here we show that additional constraints derived from a previously solved *N*MR^2 protein-analog complex structure, such as information on the location of the binding site or the assignment of one (or more) of the protein methyl groups, can be used to make the *N*MR^2 structure calculation procedure even more efficient. In the present case of the HDM2(15–111)-caylin-1 complex, the computation time could be reduced by almost two orders of magnitude compared to the initially solved HDM2(15–111)-analog *N*MR^2 complex structure. By delivering 3D-structure time-efficiently, especially for protein-analog complexes, we anticipate that*N*MR^2 will become an essential tool in structure-based drug discovery, particularly when X-ray crystallography is challenging to implement.

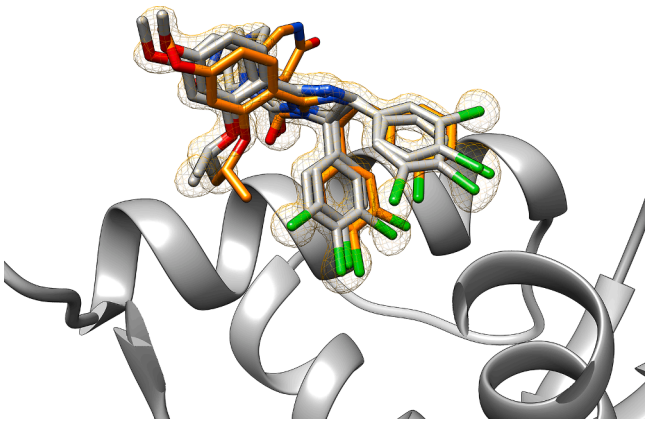

Fig. 2. Superposition of the *N*MR^2 and X-ray structures of HDM2 in complex with caylin-1. Comparison of the *N*MR^2-derived complex structure (orange) with the X-ray structures of the HDM2-caylin-1 complex (gray) and the corresponding electron density depicted in mesh grid. The overlap was created by superimposing the protein structures. The structure of caylin-1 solved by X-ray crystallography shows two equally populated conformations of the dichlorophenyl rings, one of them overlapping well with the *N*MR^2 structure. The protein is depicted with ribbons and caylin-1 using sticks with heteroatoms color-coded red for oxygen, blue for nitrogen, green for chlorine and orange or gray for carbon.

Appendices

Supporting information

Supplementary Figures S1–S4 and Table S1, assignment of the free and bound caylin-1.

Accession codes

The structure has been deposited in the PDB with accession code 7QDQ. Authors will release the atomic coordinates and experimental data upon article publication.

Author contributions

The manuscript was written through contributions of all authors. All authors have given approval to the final version of the manuscript.

Funding

This work was supported by the University of Vienna, the ETH Zurich, and the grant SNF [grant number 310030_192646] to JO.

Declaration of Competing Interest

The authors declare that they have no known competing financial interests or personal relationships that could have appeared to influence the work reported in this paper.

Supplementary materials

Supplementary material associated with this article can be found, in the online version, at doi:10.1016/j.jmro.2022.100032.

References

[1] J. Orts, M.A. Walti, M. Marsh, L. Vera, A.D. Gossert, P. Guntert, et al., NMR-based determination of the 3D structure of the ligand-protein interaction site without protein resonance assignment, J. Am. Chem. Soc. 138 (2016) 4393–4400.

[2] M.A. Walti, R. Riek, J. Orts, Fast NMR-based determination of the 3D structure of the binding site of protein-ligand complexes with weak affinity binders, Angew. Chem. Int. Ed. 56 (2017) 5208–5211.

[3] J. Orts, R. Riek, Protein-ligand structure determination with the NMR molecular replacement tool, NMR(2), J. Biomol. NMR (2020).

[4] M. Wälti, J. Orts, The NMR2 method to determine rapidly the structure of the binding pocket of a protein–ligand complex with high accuracy, Magnetochemistry 4 (2018) 12.

[5] F. Torres, D. Ghosh, D. Strotz, C.N. Chi, B. Davis, J. Orts, Protein–fragment complex structures derived by NMR molecular replacement, RSC Med. Chem. (2020).

[6] M. Wade, Y.V. Wang, G.M. Wahl, The p53 orchestra: Mdm2 and Mdmx set the tone, Trends Cell Biol. 20 (2010) 299–309.

[7] J. Kallen, A. Goepfert, A. Blechschmidt, A. Izaac, M. Geiser, G. Tavares, et al., Crystal structures of human MdmX (HdmX) in complex with p53 peptide analogues reveal surprising conformational changes, J. Biol. Chem. 284 (2009) 8812–8821.

[8] J.A. Barboza, T. Iwakuma, T. Terzian, A.K. El-Naggar, G. Lozano, Mdm2 and Mdm4 loss regulates distinct p53 activities, Mol. Cancer Res. 6 (2008) 947–954.

[9] B.T. Vu, L. Vassilev, Small-molecule inhibitors of the p53-MDM2 interaction, Curr. Top. Microbiol. Immunol. 348 (2011) 151–172.

[10] M. Oren, Decision making by p53: life, death and cancer, Cell Death Differ. 10 (2003) 431–442.

[11] S.L. Harris, A.J. Levine, The p53 pathway: positive and negative feedback loops, Oncogene 24 (2005) 2899–2908.

[12] B. Wawrzynow, A. Zylicz, M. Zylicz, Chaperoning the guardian of the genome. The two-faced role of molecular chaperones in p53 tumor suppressor action, Biochim. Biophys. Acta Rev. Cancer 1869 (2018) 161–174.

[13] L.T. Vassilev, Small-molecule antagonists of p53-MDM2 binding: research tools and potential therapeutics, Cell Cycle 3 (2004) 419–421.

[14] L.T. Vassilev, p53 Activation by small molecules: application in oncology, J. Med. Chem. 48 (2005) 4491–4499.

[15] D.C. Fry, S.D. Emerson, S. Palme, B.T. Vu, C.M. Liu, F. Podlaski, NMR structure of a complex between MDM2 and a small molecule inhibitor, J. Biomol. NMR 30 (2004) 163–173.

[16] L.T. Vassilev, B.T. Vu, B. Graves, D. Carvajal, F. Podlaski, Z. Filipovic, et al., *In vivo* activation of the p53 pathway by small-molecule antagonists of MDM2, Science 303 (2004) 844–848.

[17] Y. Zhao, A. Aguilar, D. Bernard, S. Wang, Small-molecule inhibitors of the MDM2-p53 protein-protein interaction (MDM2 Inhibitors) in clinical trials for cancer treatment, J. Med. Chem. 58 (2015) 1038–1052.

[18] A. Mullard, p53 programmes plough on, Nat. Rev. Drug Discov. 19 (2020) 497–500.

[19] W.F. Vranken, W. Boucher, T.J. Stevens, R.H. Fogh, A. Pajon, M. Llinas, et al., The CCPN data model for NMR spectroscopy: development of a software pipeline, Proteins 59 (2005) 687–696.

[20] C. Zwahlen, P. Legault, S.J.F. Vincent, J. Greenblatt, R. Konrat, L.E. Kay, Methods for measurement of intermolecular NOEs by multinuclear NMR spectroscopy: application to a bacteriophage lambda N-peptide/boxB RNA complex, J. Am. Chem. Soc. 119 (1997) 6711–6721.

[21] J. Orts, B. Vogeli, R. Riek, Relaxation Matrix Analysis of Spin Diffusion for the NMR Structure Calculation with eNOEs, J. Chem. Theory Comput. 8 (2012) 3483–3492.

[22] M. Blackledge, F. Cordier, P. Dosset, D. Marion, Precision and uncertainty in the characterization of anisotropic rotational diffusion by N-15 relaxation, J. Am. Chem. Soc. 120 (1998) 4538–4539.

[23] P. Guntert, Automated NMR structure calculation with CYANA, Methods Mol. Biol. 278 (2004) 353–378.

[24] D. Liebschner, P.V. Afonine, M.L. Baker, G. Bunkoczi, V.B. Chen, T.I. Croll, et al., Macromolecular structure determination using X-rays, neutrons and electrons: recent developments in Phenix, Acta Crystallogr. D 75 (2019) 861–877.

[25] P. Emsley, K. Cowtan, Coot: model-building tools for molecular graphics, Acta. Crystallogr. D Biol. Crystallogr. 60 (2004) 2126–2132.

[26] S. Uhrinova, D. Uhrin, H. Powers, K. Watt, D. Zheleva, P. Fischer, et al., Structure of free MDM2 N-terminal domain reveals conformational adjustments that accompany p53-binding, J. Mol. Biol. 350 (2005) 587–598.